Environmental Earth Sciences (2020) 79:432
https://doi.org/10.1007/s12665-020-09170-5

ORIGINAL ARTICLE

Modeling of methane migration from gas wellbores into shallow groundwater at basin scale

Reza Taherdangkoo[1] · Alexandru Tatomir[1,2] · Martin Sauter[1]

Received: 10 March 2020 / Accepted: 3 September 2020 / Published online: 18 September 2020
© The Author(s) 2020

Abstract

Methane contamination of drinking water resources is one of the major concerns associated with unconventional gas development. This study assesses the potential contamination of shallow groundwater via methane migration from a leaky natural gas well through overburden rocks, following hydraulic fracturing. A two-dimensional, two-phase, two-component numerical model is employed to simulate methane and brine upward migration toward shallow groundwater in a generic sedimentary basin. A sensitivity analysis is conducted to examine the influence of methane solubility, capillary pressure–saturation relationship parameters and residual water saturation of overburden rocks, gas leakage rate from the well, tilted formations, and low-permeability sediments (i.e., claystones) on the transport of fluids. Results show that the presence of lithological barriers is the most important factor controlling the temporal–spatial distribution of methane in the subsurface and the arrival time to shallow groundwater. A pulse of high leakage rate is required for early manifestation of methane in groundwater wells. Simulations reveal that the presence of tilted features could further explain fast-growing methane contamination and extensive lateral spreading reported in field studies.

Keywords Hydraulic fracturing · Methane leakage · Groundwater monitoring · Unconventional gas development · Numerical modeling

Introduction

The global demand for energy is continuously increasing around the world and the International Energy Agency (IEA) anticipated more than 25% of growth by 2040 (IEA 2018). Natural gas production from unconventional resources is considered as a promising future source for energy supply as a bridge fuel toward a low-carbon energy system (Brown et al. 2009; McGlade et al. 2013). The surge for unconventional gas development has been projected to have impact on drinking water resources (Osborn et al. 2011; Sauter et al. 2012; Vengosh et al. 2014). The most frequent and severest threats are likely associated with (1) water acquisition in dry areas, (2) leaks and spills of fracturing fluids and wastewater (i.e., flowback and produced water) at the surface, (3) discharge of inadequately treated wastewater to the environment, and (4) migration of liquids (i.e., fracturing fluids and brine) and gas from deep hydrocarbon reservoirs into shallow aquifers (Melchers 2009; Rudolph et al. 2010; Sauter et al. 2012; Kissinger et al. 2013; U.S. EPA 2015; Rice et al. 2018a; Schout et al. 2020). Of the potential mechanisms identified, the focus of this study is on fugitive gas and brine migration from a leaky natural gas well through overburden rocks towards shallow groundwater.

Natural gas is mainly composed of methane with a small amount of carbon dioxide, oxygen, nitrogen, and hydrogen sulfide. Methane in stream flows and groundwater is either of biogenic and thermogenic origin. The origin of methane can be typically assessed by geological, hydrological, and geochemical analysis (Jackson et al. 2013; Darrah et al. 2014; Siegel et al. 2015). Biogenic methane is produced by microbiological processes from in situ fermentation or reduction of carbon dioxide. Thermogenic methane is derived from the upward migration of natural gas associated with deep hydrocarbon formations (Gorody 2012; Darrah et al. 2015). Moreover, thermogenic methane has been observed to reach

✉ Reza Taherdangkoo
reza.taherdangkoo@geo.uni-goettingen.de

1 Department of Applied Geology, Geosciences Center, University of Göttingen, Goldschmidtstr. 3, 37077 Göttingen, Germany

2 Department of Earth Sciences, Uppsala University, Villavägen 16, 75236 Uppsala, Sweden

Content courtesy of Springer Nature, terms of use apply. Rights reserved.

shallow groundwater systems through anthropogenic activities such as hydraulic fracturing (Warner et al. 2012; Darrah et al. 2015). Methane does not react until dissolved in groundwater, in which case methane is rapidly being oxidized given respective redox conditions (Sherwood et al. 2016; Molofsky et al. 2016). Although methane is commonly regarded as a non-toxic substance, elevated levels of dissolved methane concentrations could change groundwater geochemistry, potentially leading to water-quality degradation (Duncan 2015; Hendry et al. 2017).

The presence of thermogenic methane in groundwater in the vicinity of oil and gas operations is most commonly associated with leakage from hydrocarbon wells (Jackson et al. 2013; Darrah et al. 2015; Rivard et al. 2019). Multiple studies have shown that leaked methane from the deep subsurface migrates upward by the buoyancy resulting from density contrasts between gas and brine (Rice et al. 2018a). Natural and anthropogenic permeable pathways such as leaky oil and gas abandoned wells, fault zones, and extensive fracture systems could facilitate the vertical movement of methane to shallow depths (Kissinger et al. 2013; Vengosh et al. 2014; Steelman et al. 2017; Yudhowijoyo et al. 2018; Tatomir et al. 2018; Riddick et al. 2019).

The quantitative analysis of the extent of methane leakage is complex even in simple geologic settings (Steelman et al. 2017; Cahill et al. 2017). Along with observational field studies, such as controlled methane-release experiments (Cahill et al. 2017), numerical modeling of subsurface flow and transport of methane plays an essential role in advancing conceptual models to be able to better evaluate the relationship between groundwater quality and hydrocarbon development. Numerical modeling could be used to address unresolved questions associated with the observational studies on fluid flow and mass transport to groundwater. A major challenge associated with numerical modeling of methane migration between deep hydrocarbon reservoirs and shallow aquifers is due to the complex nature of multiphase, multicomponent flow, and transport phenomena involved in methane leakage through a variety of geological materials, wellbores, faults, fractures, and low-permeability rocks.

The major focus of previous numerical studies was on the rapid migration of methane to groundwater through leaky wellbores, faults, and fractures (e.g., Kissinger et al. 2013; Reagan et al. 2015; Schwartz 2015; Roy et al. 2016; Rice et al. 2018b; Moortgat et al. 2018; Soltanian et al. 2018; Nowamooz et al. 2018; D'Aniello et al. 2019), while less effort was directed at understanding the slow migration through overburden rocks (Nowamooz et al. 2015) as well as the influence of methane solubility on transport (Soltanian et al. 2018; Schout et al. 2020). In this study, we investigate the migration of free- and dissolved-phase methane from a leaky natural gas well to groundwater through overburden sediments at the basin scale. We specifically focus on the role of low-permeability sediments, tilted formations, and methane leakage rates and periods on the transport of methane to shallow subsurface.

We start with a generic conceptual model derived from an FEP knowledge database and the expert ranking of the key features, events, and processes that generate failure scenarios at basin scale (Tatomir et al. 2015, 2018). From the conceptual model, we build two-dimensional two-phase, two-component numerical models to study the flow and transport of methane and brine from a leaky gas well into groundwater for 25 years. The horizontal model domain has 1800 m depth and 10 km width. First, we evaluate the impact of methane solubility on fluid migration dynamics and the leakage rates into shallow subsurface. Then, we examine the influence of (1) the parameters describing capillarity pressure and relative permeability saturation of shallow and overburden rocks, (2) the low-permeability sediments, (3) the tilted formations (up to 3°), and (4) the methane leakage rate from the gas well. Finally, we compare the modeling results with the findings of observational studies.

Materials and methods

Conceptual model for methane and brine migration at the basin scale

We build a generic basin-scale two-dimensional numerical model, Fig. 1, comprising three horizontal layers. The conceptual model is built based on permeability and stratigraphy data compilations of North America and Europe implemented by Taherdangkoo et al. (2018) and Potter van Loon (2016). We applied median values reported for the domain length, recharge, claystone thickness, and claystone depth. A thin (21 m) continuous claystone is assumed at shallow depth (171 m) overlain by coarse sediments. The model spans across a domain of 10 km length and 1.8 km depth.

A large section of the top boundary, i.e., 95% of the model length, is defined as a constant recharge boundary intersecting a discharge boundary (5% of the model length). The groundwater recharge rate amounts to 0.05 m/year. The discharge is modeled as a constant hydraulic head boundary (Taherdangkoo et al. 2018). The lateral sides of the domain are set to no-flow boundaries.

It is common in the oil and gas industry to temporarily shut-in a well because of operational and economic reasons. The pressure in the gas reservoir does not decrease during the shut-in period. For this type of condition, should the well annulus intersect with a fracture/fracture system connecting the gas reservoir with the overburden, considerable leakage may occur (Reagan et al. 2015; Moortgat et al. 2018; Tatomir et al. 2018). The leakage rate depends on various factors such as reservoir pressure, reservoir gas saturation,

Content courtesy of Springer Nature, terms of use apply. Rights reserved.

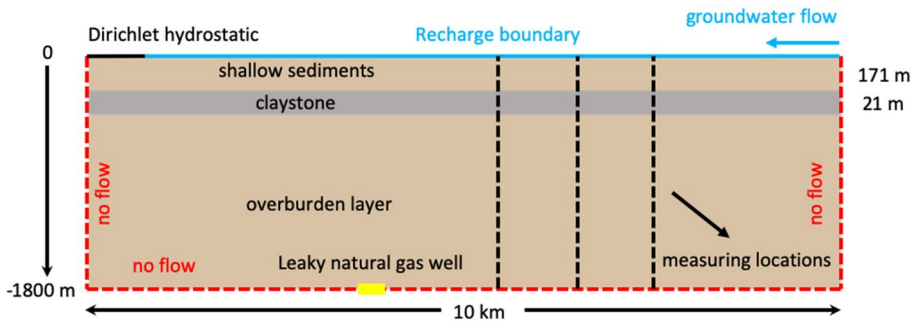

Fig. 1 Generalized conceptual model of methane and brine migration from the gas reservoir into the overlying formations for the base-case model. The low-permeability layer, i.e., claystone, is indicated in gray and permeable sediments in light brown. The black dashed lines represent the monitoring locations at distances $\Delta = 2000$ m, 3000 m, and 4000 m from the leaky gas well. The leakage area is presented in yellow. Groundwater flow is from right to left, and the discharge area is modeled as a Dirichlet boundary condition

in situ, and relative permeability (Reagan et al. 2015; Nowamooz et al. 2015). Kissinger et al. (2013) modeled constant leakage of methane from the reservoir into the overburden for 100 years. The authors emphasized that the constant escape of gas is regarded as "a conservative" assumption. Reagan et al. (2015) suggested that incidents of gas leakage from the reservoir are likely to be limited in time. Moortgat et al. (2018) considered a high methane inflow rate during the shut-in period, followed by a lower rate during the production.

The conceptual model considered here assumes fracture propagation into overlying formations during a hydraulic fracturing treatment (Kissinger et al. 2013; Reagan et al. 2015; Moortgat et al. 2018; Tatomir et al. 2018). The model assumes that during shut-in gas leaks into the overburden at a high flow rate, followed by a much lower rate once the production is resumed. We applied leakage rates published in Moortgat et al. (2018) as, similar to this study, they assumed methane leakage from a natural gas well into overlying formations. However, the geological setting, rock types, and tectonics are different from those considered here.

The leakage is assumed to occur at the top of the gas reservoir through the fracture system intersecting the overburden; thus, instead of explicitly considering the reservoir in the model, it is included as a boundary condition. The gas entering the domain is assumed to be pure methane and the presence of other thermogenic gases is neglected (Nowamooz et al. 2015; Roy et al. 2016; Rice et al. 2018a). The leakage source measures 100 m in length and it is situated at the bottom of the domain at 40% of the model length ($3950 \leq x \leq 4050$) for all subsequent simulations. The remaining of the lower boundary is set to no-flow condition. The methane leakage rate is estimated based on the production rate from the borehole. A typical production rate of 300 MSCFD (million standard ft^3/day) (Moortgat et al. 2018) (35,680 m^3/day at reservoir condition) is assumed for the base-case model. Methane leaks into the overburden at a high inflow rate of 8920 m^3/day, i.e., 25% of the production during the 7 days of the shut-in period, followed by an inflow rate of 892 m^3/day, i.e., 10% of the initial leakage rate, for the next 2 years. The upward migration of methane and brine is monitored for 25 years of simulation time.

The low-permeability unit, i.e., claystone, is a laterally extensive single layer overlying the entire basin which might contain discontinuities. Moreover, multi-layered systems where low-permeability units are interbedded within permeable sediments may exist. Each field configuration could lead to a different contamination distribution in the subsurface based on its unique stratigraphic, geophysical, and hydrodynamic characteristics (Sauter et al. 2012; Lange et al. 2013). Herein, we first assume a single continuous claystone across the entire model length to obtain the first-order information on the influence of low-permeability sediments on methane migration. We then consider different configurations to explore the impact of claystone integrity and multi-layered clay systems.

Numerical modeling approach

The dominant physical and chemical processes for fluid migration are advection (viscous, buoyant, and capillary), dissolution, and diffusion (Nowamooz et al. 2015). Methane sorption is assumed to be negligible (Rice et al. 2018b). The flow and transport of fluids are simulated using both a miscible flow model and an immiscible flow model. The miscible flow model considers advection, diffusion, and dissolution processes, while the immiscible model considers migration via advection and diffusion.

All simulation runs are conducted with the open-source numerical simulator DuMu^X (Flemisch et al. 2011). For spatial discretization, the box method, a vertex (or node)-centered finite volume method based on a finite-element grid, is used. The grid resolution equals 500 cells in the x-direction and 180 cells in the y-direction, corresponding

Content courtesy of Springer Nature, terms of use apply. Rights reserved.

to finite volume element length of 20 m in x-direction, and 10 m in y-direction. A fully implicit Euler time discretization scheme using the Newton method is applied to solve the linearized system of non-linear partial differential equations (Helmig 1997). The first time-step size is set to 0.01 s and the maximum time-step is 1e6 s. The time-step size is controlled by the number of iterations required by the Newton method to achieve convergence for the last time integration (Flemisch et al. 2011; Koch et al. 2020).

We use 2P2C (two-phase, two-component) and 2P (two-phase) modules for simulating isothermal miscible and immiscible two-phase flow and transport of fluids in porous media, respectively. The binary diffusion and the diffusive mass fluxes in each phase are computed according to Fick's law. The mass balance equation for a two-phase two-component model can be formulated for each k as follows (Helmig 1997; Dietrich et al. 2005):

$$\frac{\partial\left(\emptyset \sum_{\alpha} \rho_{\alpha} X_{\alpha}^{k} S_{\alpha}\right)}{\partial t} - \sum_{\alpha} \nabla \cdot \left\{ \rho_{\alpha} X_{\alpha}^{k} \frac{k_{r\alpha}}{\mu_{\alpha}} \boldsymbol{K}\left(gradP_{\alpha} - \rho_{\alpha}\boldsymbol{g}\right) + \rho_{\alpha} D_{pm,\alpha}^{k} gradX_{\alpha}^{k} \right\} - q^{k} = 0, \quad (1)$$

$$\alpha \in \{w, n\} \; and \; k \in \{brine, methane\}$$

where the index α represents the wetting and non-wetting phases. The index κ represents the components brine and methane. φ is the effective porosity and ρ_{α} is the density of phase α. X_{α}^{k} is the mass fraction of component κ in the phase α, S_{α} is the saturation, μ_{α} is the dynamic viscosity, and $k_{r\alpha}$ is the relative permeability. $\boldsymbol{K}$ is the intrinsic permeability tensor, P_{α} is the phase pressure, **g** is the gravitational acceleration, and $D_{Pm,\alpha}^{k}$ is the effective diffusion coefficient of the porous medium.

Methane can exist as a free-phase gas with a limited amount of water vapor or dissolved in the aqueous phase. The amount of water in the gas phase based on Duan et al. (1992a). Methane solubility varies over a wide range of temperatures, pressures, and brine compositions (Duan et al. 1992a; Duan and Mao 2006). Methane dissolution in the aqueous phase is assumed to occur at thermodynamic equilibrium and gas-phase saturations were simultaneously updated at each time-step to consider the mass loss to brine. Assuming methane at equilibrium with respect to water, methane solubility (mg/L) can be computed following the Duan et al. (1992a) approach as in:

$$ln\frac{x_{CH_4}P}{m_{CH_4}} = \frac{\mu_{CH_4}^{l(0)}}{RT} - ln\emptyset_{CH_4} + \sum_{c} 2\lambda_{CH_4-c} m_c + \sum_{a} 2\lambda_{CH_4-a} m_a + \sum_{c}\sum_{a} \zeta_{CH_4-c-a} m_c m_a, \quad (2)$$

where m is the molality of CH_4 or salts in the liquid phase and x is the composition in the vapor phase. P is the total pressure and R is the universal gas constant. $\mu_{CH_4}^{l(0)}$ is the standard chemical potential of CH_4 in the liquid phase and Ø is the fugacity coefficient. The index a and c are anion and cation, respectively. λ_{CH_4-ion} and ζ_{CH_4-c-a} are interaction parameters. $\frac{\mu_{CH_4}^{l(0)}}{RT}$ and the interaction parameters are calculated by Pitzer et al. (1984) method (Duan et al. 1992a).

Material properties

The variations in porosity and permeability are typically driven by changes in mineralogical composition, i.e., mineral grains and cement, depositional facies, burial depth, and post-depositional processes (Weibel et al. 2012). The mineral composition of the claystone comprises 50% kaolinite and 50% illite (Luijendijk and Gleeson 2015). Following Gleeson et al. (2011), we assumed that the shallow and overburden sediments contain 90% sand and 10% clay and obtained realistic permeability values. The permeability of sand is calculated using the Kozeny–Carman equation (Kozeny 1927; Carman 1937). The claystone permeability is determined using an empirical permeability-void ratio equation (Luijendijk and Gleeson 2015). The permeability of sediments is calculated following Luijendijk and Gleeson (2015). The porosity is calculated using lithology dependent exponential porosity-depth coefficients (Athy 1930; Sclater and Christie 1980). The estimated porosity and vertical permeability of claystone are 0.05 and 1.1×10^{-20} m^2, respectively (Fig. 2). Permeability and porosity of shallow and overburden sediments in the y-direction vary approximately from 6.8×10^{-14} to 2.6×10^{-15} m^2 and from 0.3 to 0.12, respectively, as shown in Fig. 2. The anisotropy ratio (K_h/K_v) is set to 100 in the claystone and 10 in the surrounding sediments. The temperature at the top of the domain is 10 °C, with a vertical temperature gradient of 0.03 °C/m. The domain is initially water-saturated. The residual water saturation is set to 20% (Nowamooz et al. 2015; Rice et al. 2018b). In all simulations, we modeled a drainage-like process, because the gas saturation increases continuously with time. As gas cannot be trapped during the drainage, the residual gas saturation is assumed to be 0.01% (Rice et al. 2018b).

Methane is the predominant component in the gas mixture and small amounts of other components (e.g., N_2, CO_2, C_2, and C_3) have a negligible influence on the density and viscosity of the gas phase (Nowamooz et al. 2015). For simplification, the model considers the leaked gas as pure methane. Brine is modeled as a pseudo-component and represents pure water with a given salinity. Brine density and viscosity are calculated following Batzle and Wang (1992) equations. Methane density and viscosity are calculated based on Duan

Content courtesy of Springer Nature, terms of use apply. Rights reserved.

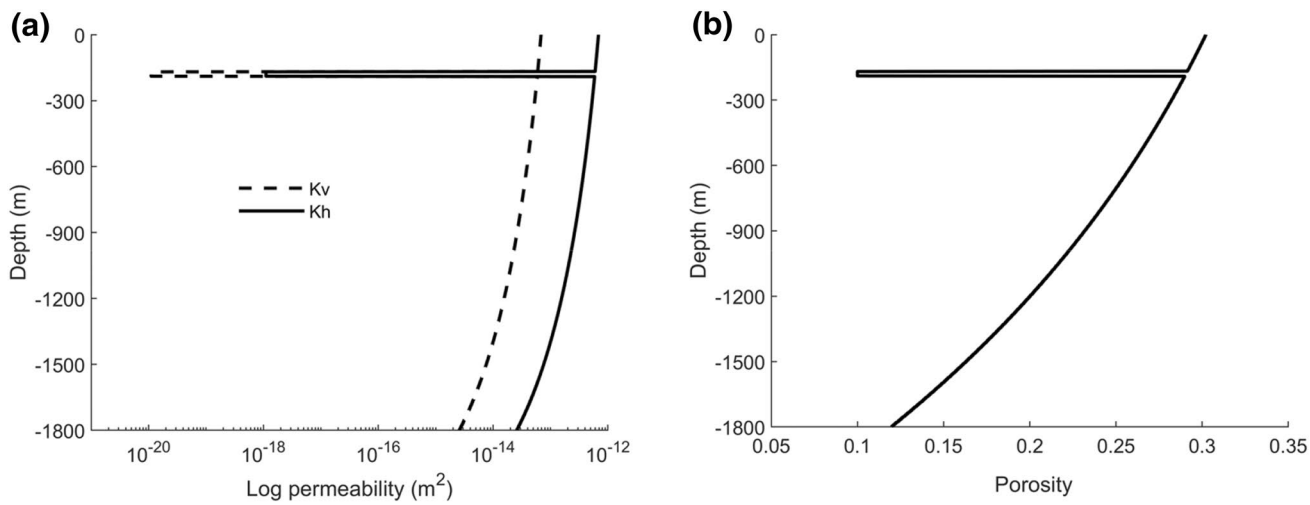

Fig. 2 Distribution of **a** permeability and **b** porosity in the domain

et al. (1992b, c) and (Daubert et al. 1998), respectively. The diffusion coefficient of water in the gas phase is calculated based on Fuller et al. (1966). Since the empirical equations for estimating the diffusion coefficient in infinite solution presented in Reid et al. (1987) all show a linear dependency on temperature, we simply scale the experimentally obtained diffusion coefficient of the dissolved methane in the water phase given in Kobayashi (2004) by temperature. Kobayashi (2004) suggested the diffusion coefficient of 3.55×10^{-9} m^2/s.

As methane leakage rates reported by Moortgat et al. (2018) are specified for surface conditions, a gas formation volume factor (B_g) of 0.0042 ft^3/SCF is used to convert the values to reservoir conditions. The B_g is calculated using the averaged values reported by Edwards and Celia (2018). The model property values are presented in Table 1. The capillary pressure and the relative permeability are calculated as a function of saturation using Brooks and Corey (1964) equations as follows:

$$P_c = P_d S_e^{\frac{-1}{\lambda}}, \tag{3}$$

where P_d is the entry pressure of the porous medium. The relative permeability functions, $K_r(S)$, can be calculated by the following equations:

$$K_{rw} = S_e^{\frac{2+3\lambda}{\lambda}}, \text{ for the wetting phase} \tag{4}$$

$$K_{rg} = \left(1 - S_e\right)^2 \left(1 - S_e^{\frac{2+\lambda}{\lambda}}\right), \text{ for the non-wetting phase.} \tag{5}$$

The effective saturation S_e is defined using the following equation. S_{wr} and S_{gr} are irreducible saturation of liquid and gas phases, respectively:

$$S_e = \frac{S_w - S_{wr}}{1 - S_{gr} - S_{wr}}. \tag{6}$$

Simulation strategy

The base-case models explore miscible and immiscible flow and transport of fluids to shallow layers for a period of 25 years. The temporal and spatial behavior of the plume in the subsurface and the change in volumetric flow rates to shallow groundwater of methane are observed. Moreover, methane and brine flow rates at various distances from the leaky gas well ($\Delta L = 2000$, 3000, and 4000 m) are monitored. These locations can be interpreted as intersections of the aquifer with conductive permeable pathways such as faults and fractures, i.e., preferential flow paths for the transport of fluids in the upper crust. This choice allowed us to track the methane plume at various distances from the gas wellbore in basins with or without vertical permeable pathways.

A series of sensitivity analyses is designed to examine the roles of different geometric configurations and parameter combinations on the migration of fluids. Parameter selection is based on comprehensive features, events, and processes (FEPs) procedure highlighting the relevant importance of the key factors influencing the upward movement of contaminants (Tatomir et al. 2018). First, we explore the sensitivity of hydrodynamic properties (P_d, λ, and S_{wr}) of shallow and overburden sediments. The displacement or entry pressure (P_d) of the porous medium changes between 2 and 20 kPa and is set to 10 kPa in the base-case model. A large pore size distribution index (λ) indicates a comparatively uniform pore size distribution, while small values of λ describe a non-uniform distribution (Brooks and Corey 1964). λ varies

Content courtesy of Springer Nature, terms of use apply. Rights reserved.

Table 1 Parameter values used in the base-case model and the variation range for the sensitivity analysis

Parameter	Unit	Base-case value	Range of variation
Compressibility of solid phase	Pa^{-1}	4.5×10^{-10}	
Recharge at the top boundary	m/year	0.05	
Temperature at the top boundary	°C	10	
Temperature gradient	°C/m	0.03	
Gas formation volume factor	ft^3/SCF	0.0042	
Methane density at atmospheric condition	kg/m^3	0.72	
Entry pressure of the claystone	kPa	12	
Entry pressure of the surrounding sediments	kPa	10	2–20
Brooks-Corey parameter		2.0	2–6
Residual gas saturation		0.0001	
Residual water saturation		0.2	0.15–0.25
Permeability of the claystone	m^2	1.1×10^{-20}	
Porosity of the claystone		0.05	
Permeability of the surrounding sediments	m^2		2.6×10^{-15} to 6.8×10^{-14}
Porosity of the surrounding sediments			0.12–0.3
Anisotropy ratio in the claystone		100	
Anisotropy ratio in the surrounding sediments		10	

from 2 to 6 and is set to 2 in the base-case model. These values are chosen to cover a wide range of values of pore size distribution index and entry pressure. Residual water saturation varies between 0.15 and 0.25 and equals to 2.0 in the base-case model (Class 2007; Nowamooz et al. 2015; Rice et al. 2018b).

We include simulations for sedimentary basins with dip angles of 0º, 1º, and 3º. We rotate the model coordinate system to tilt the geological geometric configuration. We keep the top of the domain at the same depth and increase the maximum depth by increasing the dip. Thereafter, the impact of methane leakage rate from the wellbore is explored. As an alternative to the high leakage with short duration, two low constant gas inflow rates of 60 and 120 m^3/day for uninterrupted 25 years are considered.

The sensitivity analysis then considers a discontinuity, 10% of the model length, in the middle of the claystone to examine the role of low-permeability rocks on fluid flow and mass transport. Further simulations include the integration of a multi-layered claystone system with interbedded permeable rocks at shallow depth. We assume two different field settings by varying the geometry of the clay system, consisting of four clays with random horizontal position, depth, and integrity. All clays are embedded between 150 and 350 m depth and have the same thickness as the base-case value, 21 m. This sensitivity analysis is presented to examine how the migration of methane from a deep gas reservoir is impacted by sequences of low-permeability rocks.

Results and discussion

Base-case model

The gas saturation and pressure profiles of methane leakage using the miscible flow model are shown in Figs. 3 and 4, respectively. In this model, methane exists as free and dissolved-phase gas in the aqueous phase. Methane migrates upward predominantly by buoyancy and reach the claystone after approximately 695 days. The strong vertical buoyancy controls the direction of methane migration; thus, the lateral spread is limited. The tube-shaped flow of gas is partially due to the consideration of a homogenous model domain. The diameter of the plume around the leakage source is approximately 320 m after 2 years and remains constant. The claystone overlying the overburden sediments constitutes an effective barrier to the upward movement of fluids. For this type of configuration, once methane reaches the claystone layer, the gas spreads laterally along the horizontally stratified layer due to the sustained pressure. As illustrated in Fig. 5, an important volume of gas phase accumulates at the claystone base after 25 years reaching eventually the aquifer. Permeable pathways, such as fractures, faults, and abandoned wells through barrier rocks, play an important role in fluid migration in the upper crust. In the context of hydraulic fracturing operations, the presence of these flow paths in the proximity of a leaky gas well could lead to the early occurrence of methane in groundwater (Darrah et al. 2014; Cahill et al. 2017; Moortgat et al. 2018).

For the time 25 years after the leakage, the dissolved methane (mg/L) in the aqueous phase is presented in Fig. 5b.

Content courtesy of Springer Nature, terms of use apply. Rights reserved.

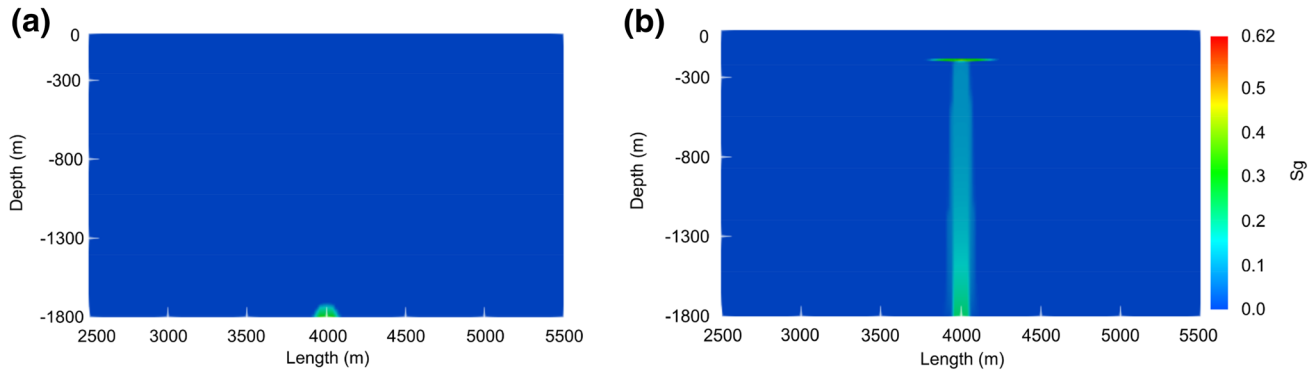

Fig. 3 Gas-phase saturation profiles after **a** 7 days and **b** 2 years of methane leakage into the overburden formations. The employed model assumes miscible flow and transport of fluids

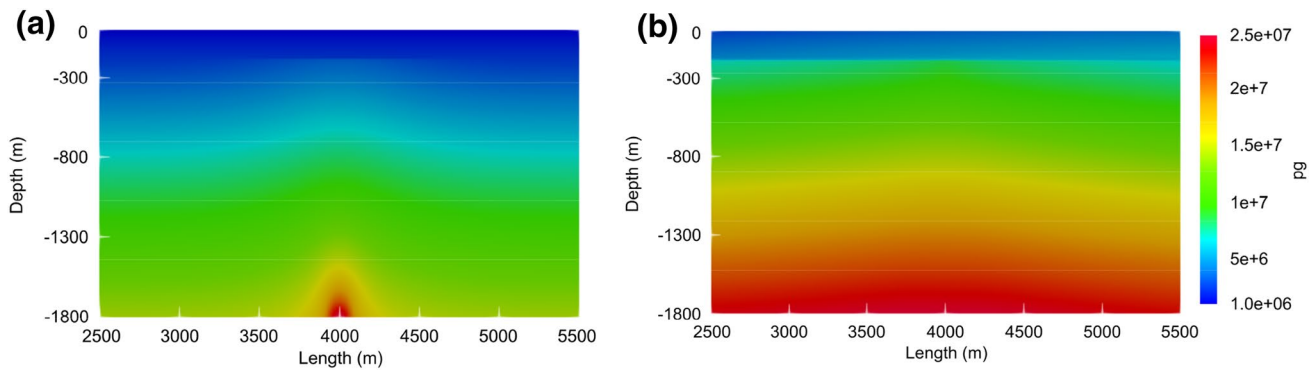

Fig. 4 Pressure profiles after **a** 7 days and **b** 2 years of methane leakage into the overburden formations. The employed model assumes miscible flow and transport of fluids

The density of the gas phase and the composition of the aqueous phase strongly depend on pressure and temperature. Methane solubility in the aqueous phase is higher in deep formations due to the increase in pressure (Eq. 2), and thus, more methane is dissolved in brine before the appearance of the gas phase (Duan et al. 1992a; Duan and Mao 2006). Following the commencement of leakage, free-phase methane moves upward by buoyancy and progressively dissolves in brine. Dissolved methane is gradually transported by advection and diffusion. The high buoyancy force from density contrasts between methane (density > 110 kg/m^3) and brine (density > 1100 kg/m^3) controls the long-term upward migration of free-phase methane.

As illustrated by the pressure profiles (Fig. 4), the hydrostatic pressure is lower at shallow depth. The reduction of the hydrostatic pressure leads to a significant decrease in the density of the gas phase, and the release of some of the dissolved methane into the gas phase. Accordingly, more highly buoyant free-phase methane appears at shallow depths with the consequence of increasing the upward flow rate. For such conditions, large amounts of free-phase methane migrate to the groundwater system within a relatively short time.

The gas-phase saturation and pressure profiles of the immiscible flow model are shown in Figs. 6 and 7, respectively. Methane reaches the base of the claystone after approximately 660 days. The methane accumulation at the claystone is followed by the extensive horizontal spreading. Similar to the methane migration in the miscible flow model set-up, the diameter of the plume around the leakage source measures approximately 320 m after 2 years and remains unchanged. In both miscible and immiscible flow models, the lateral spread of the plume before reaching the claystone is limited, partially due to the assumption of a homogenous domain.

The mass flow rates of methane and brine are obtained from the total non-wetting phase and wetting phase flow rates calculated from advection, diffusion, and dissolution processes. Figure 8a, b represents methane and brine volumetric flow rates at 2000, 3000, and 4000 m distances to the gas well, respectively. Methane reaches the monitoring locations during the extensive lateral spreading at the

Content courtesy of Springer Nature, terms of use apply. Rights reserved.

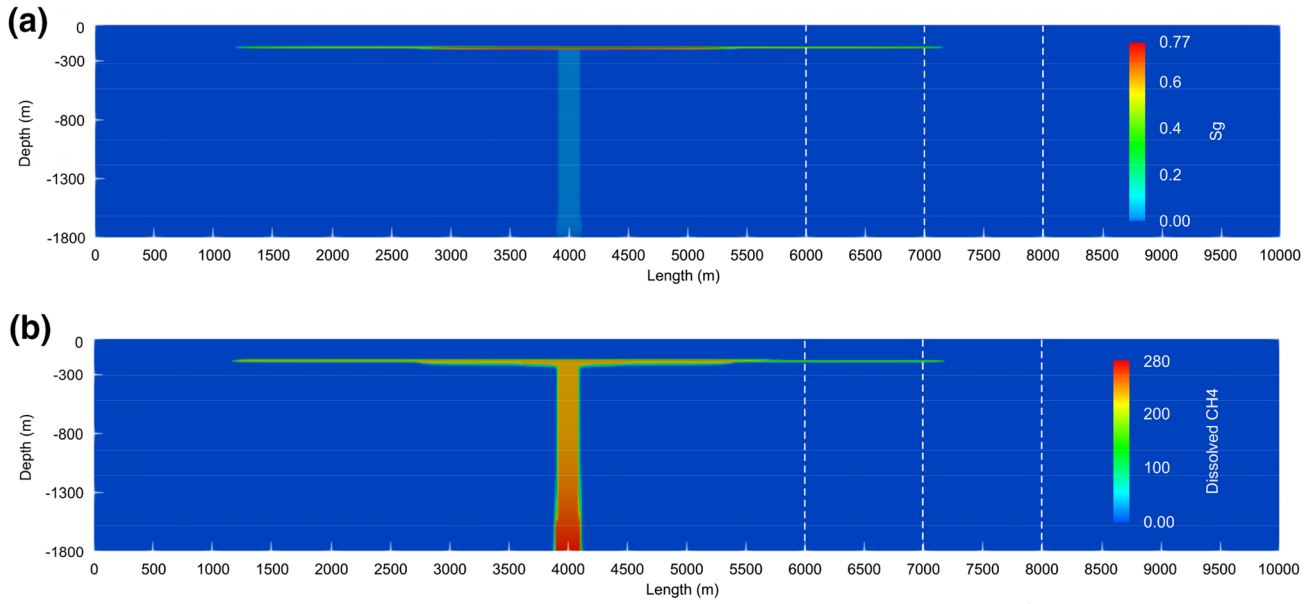

Fig. 5 Spatial distribution of **a** gas-phase saturation and **b** dissolved methane (mg/L) in the aqueous phase after 25 years of methane leakage into the overburden formations. The white dashed lines show the monitoring locations

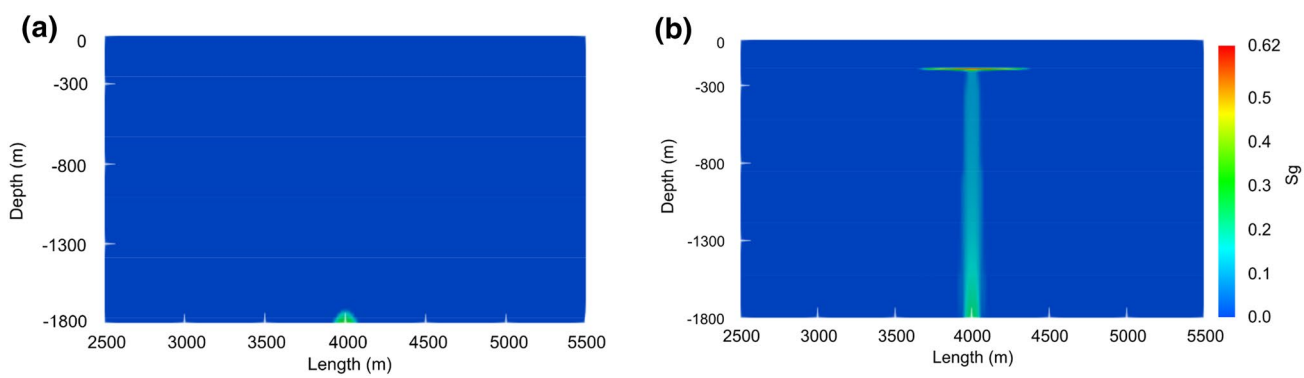

Fig. 6 Gas-phase saturation profiles after **a** 7 days and **b** 2 years of methane leakage into the overburden formations. The employed model assumes immiscible flow and transport of fluids

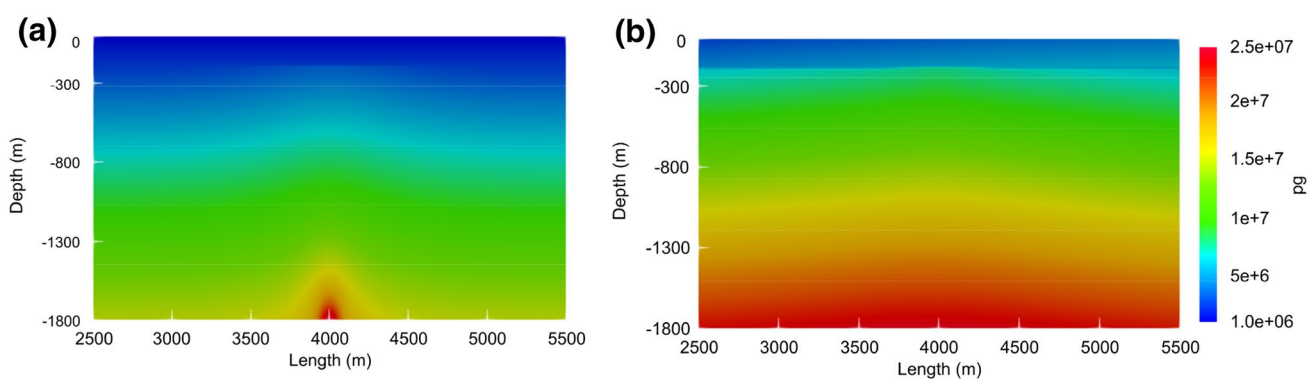

Fig. 7 Pressure profiles after **a** 7 days and **b** 2 years of methane leakage into the overburden formations. The employed model assumes immiscible flow and transport of fluids

Content courtesy of Springer Nature, terms of use apply. Rights reserved.

claystone base. The methane flow rate increases rapidly to its maximum value and then shows a continuous decrease with time (Fig. 8a). The flow rates of fluids corresponding to the miscible model are slightly lower compared to the immiscible model, indicating the effect of gas dissolution on transport. Similar to the observations of Tatomir et al. (2018), the methane flow rate is higher where the conductive feature, e.g., fault, is closer to the leakage location. However, leakage continues to be active for much longer time periods when the conductive features are further located.

The pressure gradient created by the gas influx causes brine to slowly migrate in the subsurface (Fig. 8b). Brine flow rate at the measuring locations increases during the leakage and declines sharply after the drop-in pressure. The first peak value corresponds to the end of the shut-in period and the second peak corresponds to the end of leakage. Brine flow changes in the direction of regional groundwater flow after approximately 5 years due to the combined influence of regional hydraulic gradient, cease of gas leakage, and negative buoyancy. Although brine flows towards the monitoring locations (i.e., highly permeable pathways), the probability of deep brine reaching shallow groundwater is low (Osborn et al. 2011; Gassiat et al. 2013; Pfunt et al. 2016; Taherdangkoo et al. 2019) due to the absence of significant driving forces.

As illustrated by Figs. 3, 4, 5, 6, 7, and 8, using miscible and immiscible flow models results in slightly different methane plume sizes and travel times to groundwater. This is due to the low solubility of methane in the ambient water, particularly at shallow depths. The influence of methane solubility on gas transport becomes less significant once the plume spreads at shallow groundwater.

Sensitivity analysis

The sensitivity analysis is conducted employing the miscible flow model. First, the influence of key parameters including Brooks–Corey parameters, residual water saturation, tilted geometries, and methane leakage rates are examined. Then, the impacts of the claystone integrity and multi-layered claystone systems on the spatial distribution of the methane plume in the subsurface and the arrival time to shallow groundwater are discussed.

Geological and hydrogeological parameters

The impacts of hydrodynamic properties (i.e., P_d, λ, and S_{wr}) of the shallow and overburden sediments on the transport of methane are illustrated in Fig. 9a–c. The entry pressure in the capillary pressure function is inversely correlated with methane flow rate at the monitoring locations. A higher entry pressure requires a higher non-wetting phase (i.e., gas phase) pressure to displace the ambient water resulting in the reduction of methane flow rates, as shown in Fig. 9a. The change of entry pressure has a substantial influence on the flow rate when P_d is varied over a large range.

The pore size distribution index (λ) is a shape parameter in the capillary pressure—relative permeability—saturation relationships, and has influence on the phase saturation. An inverse relationship between λ and methane flow rate is observed as an increase in the λ value increases the degree of saturation of the water phase. Varying λ within a small range has negligible impacts on arrival times and flow rates of methane, while the influence of varying λ over a wider range is noticeable.

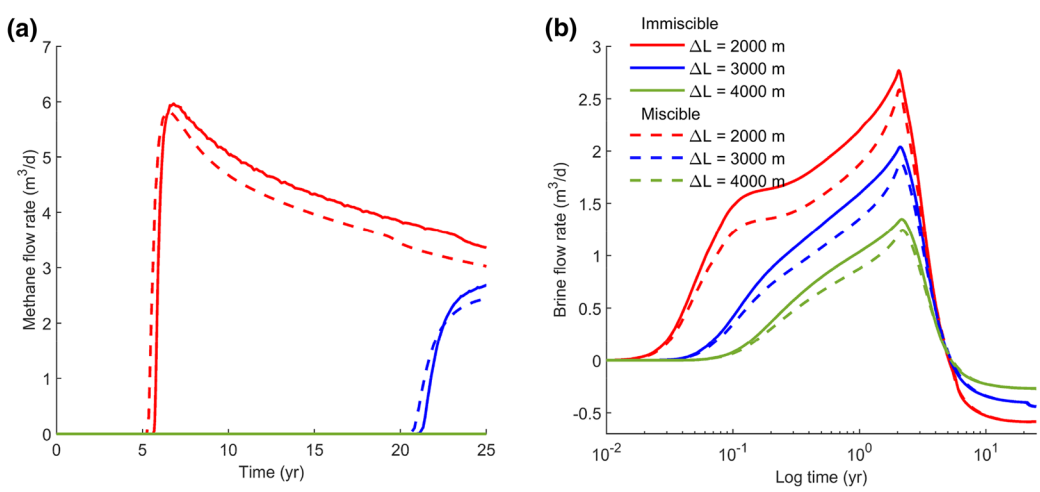

Fig. 8 **a** Methane and **b** brine flow rates at monitoring locations at distances Δ = 2000 m, 3000 m, and 4000 m from the leaky gas well for immiscible and miscible flow models

Content courtesy of Springer Nature, terms of use apply. Rights reserved.

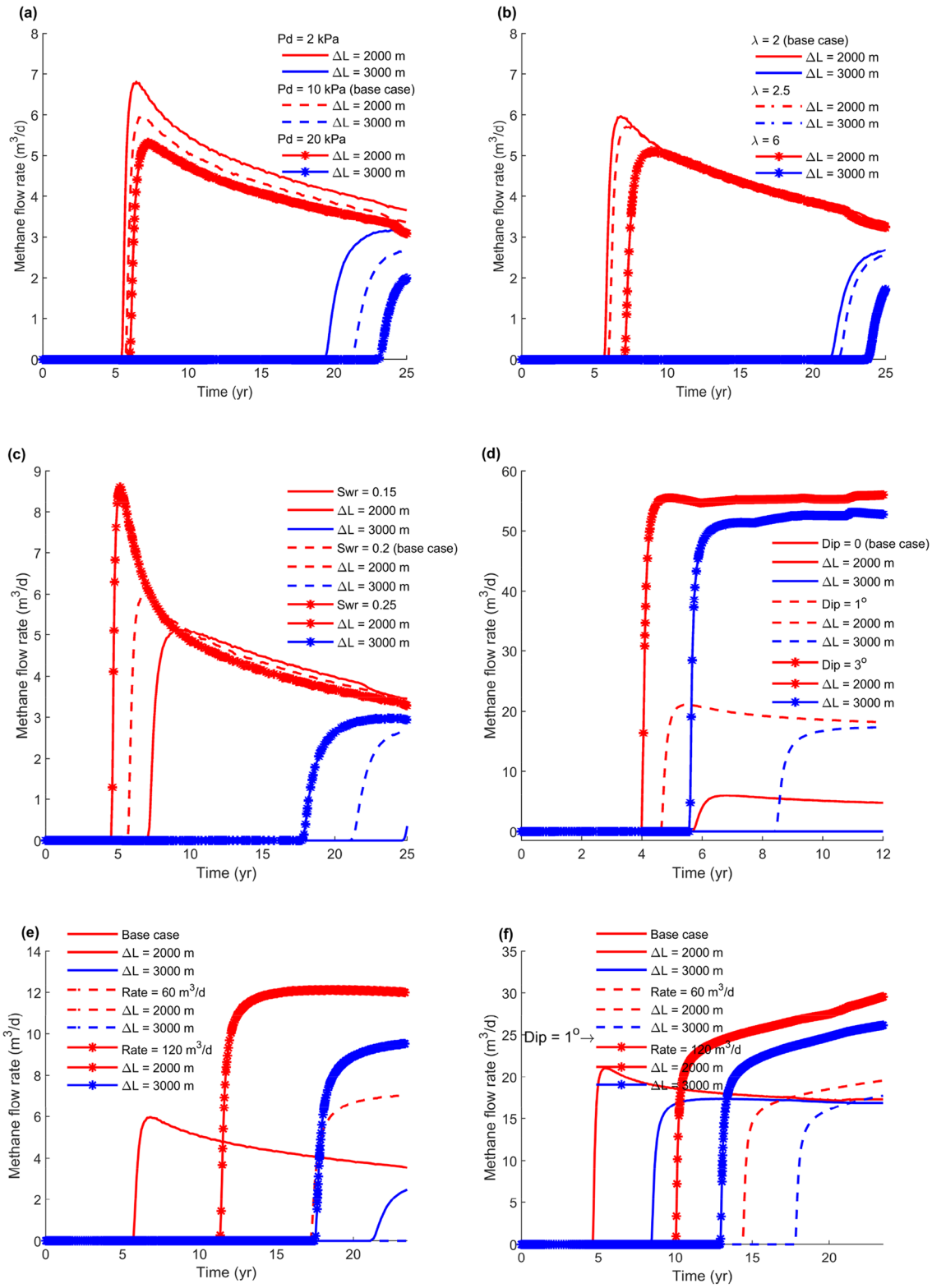

Fig. 9 Methane flow rates at the monitoring locations at distances $\Delta = 2000$ m and 3000 m from the leaky gas well for the miscible flow model varying: **a** entry pressure, **b** pore size distribution index, **c** residual water saturation, **d** tilt of formation, **e** methane inflow rate, and **f** methane inflow rate in a formation with 1° tilt

Content courtesy of Springer Nature, terms of use apply. Rights reserved.

Residual water saturation (S_{wr}) is important with respect to its influence on the relative permeability. A positive correlation between S_{wr} and methane flow rates is observed as an increase in the value of S_{wr} decreasing the amount of gas phase trapped in the pore spaces. The effects of varying S_{wr} on breakthrough time and volume of methane reaching monitoring locations are more substantial in our models in contrast to variations in P_d and λ.

In a sedimentary basin with a larger dip angle (dip ≥ 3°), the lateral buoyancy component further contributes to the horizontal spreading of the plume. Methane moves up-dip along tilted layers and spreads over a large distance from the leaky wellbore. The lateral transport distances of methane are significantly higher even for only minor tilt (1°) as compared to a horizontal domain. In the formation with 3° tilt in the *x*-direction, methane reaches the monitoring location 4000 m away from the gas wellbore within 7.2 years, but it does not spread that far in the horizontal dimension (Fig. 9d). The results suggest that the presence of tilted formations/layers can encourage the lateral spread of the plume; thus, methane can be manifested at monitoring locations even at distances of several kilometers from a leaky gas well.

Methane leakage rate from the wellbore

The pulse of high leakage rates assumed in the base-case model was compared with the continuous slow leakage of methane. The lowest gas inflow rate, i.e., 60 m^3/day, results in a delayed arrival of fluids at the monitoring locations in contrast to other cases, clearly showing less spatial spreading. The plume size is, as expected, larger with longer exposure to the leakage. Persistent long-term leakage leads to high methane concentrations in shallow layers, which induces higher contamination risks to groundwater aquifers. A pulse of high leakage rate is required to generate a larger plume and methane manifestation in shallow groundwater within short times. As illustrated in Fig. 9e, leakage rate and leakage period have significant impacts on the propagation of the plume in the overburden and accumulated methane volume in shallow groundwater.

Varying gas inflow rates in a tilted formation (~ 1°) (Fig. 9f) has significant influence on the temporal and spatial distribution of the plume in the overburden. The persistent leakage in a tilted formation leads to the extensive spreading in the direction of the tilt enhancing the risk to groundwater within a short-time scale, particularly with the presence of permeable pathways within this range. Under these conditions, free- and dissolved-phase methane could affect a larger area and millions of kilograms of methane are most likely to be transported to the aquifer. This scenario indicates that gas leakage in a tilted formation pose additional risk to shallow groundwater, partly due to the increase of lateral methane migration.

Claystone layer characteristics

We assumed a discontinuity in the center of the claystone at the location $4500 \leq x \leq 5500\,m$, to assess the influence of barrier layer integrity on the vertical movement of fluids. Methane migrates upward from the leakage source and accumulates at the claystone base. The trapped methane is compressed with the increase of pressure and tends to move upward through permeable pathways, e.g., fractures, and discontinuities. Once methane reaches the discontinuity, it preferentially migrates vertically along sediments with higher permeabilities (Fig. 10a). The low pressure and temperature at shallow depths have strong impacts on the density of the free-phase gas and its solubility in the aqueous phase; subsequently, fast vertical migration above the claystone formation slows the lateral spreading. Methane enters shallow groundwater after 2.4 years at a flow rate of 26.15 m^3/day and peaks at 3.3 years at a flow rate of 26.15 m^3/day (Fig. 11).

The impact of clay sequences is evaluated by considering two different field configurations (see the top panels in Fig. 10b, c). Each multi-layered claystone formation comprises four thin clay layers embedded in permeable sediments. The claystone layers have random horizontal position, integrity, and depth. In case I (Fig. 10b), and methane migrates upward until it is trapped by the claystone and spreads laterally in the direction of groundwater flow. The plume then flows upward from the left edge of the upper parts of the clay sequence because of the lack of an effective impermeable layer. Methane reaches the aquifer base after 4.8 years with a flow rate of 4.41 m^3/day. The plume evolution in case II (Fig. 10c) is somewhat similar to case I. Methane migrates predominantly in the direction of groundwater flow, after being deviated by the claystone sequence. The methane plume arrives at the aquifer base after 3.7 years with a flow rate of 1.01 m^3/day.

As illustrated in Fig. 11, continuous thin claystone layers constitute major safeguards against leakage of methane (free and dissolved phase) to shallow aquifers. Time to breakthrough and methane flow rate to the aquifer depend on the integrity of the claystone and the positions of discontinuities with respect to the leaky gas well. The sequence of claystone layers strongly controls the temporal and spatial behavior of the plume in the subsurface and cumulative volume of methane reaching the shallow groundwater.

Comparison with field studies

The occurrence of thermogenic methane in groundwater may indicate that the gas has migrated upward from a

Content courtesy of Springer Nature, terms of use apply. Rights reserved.

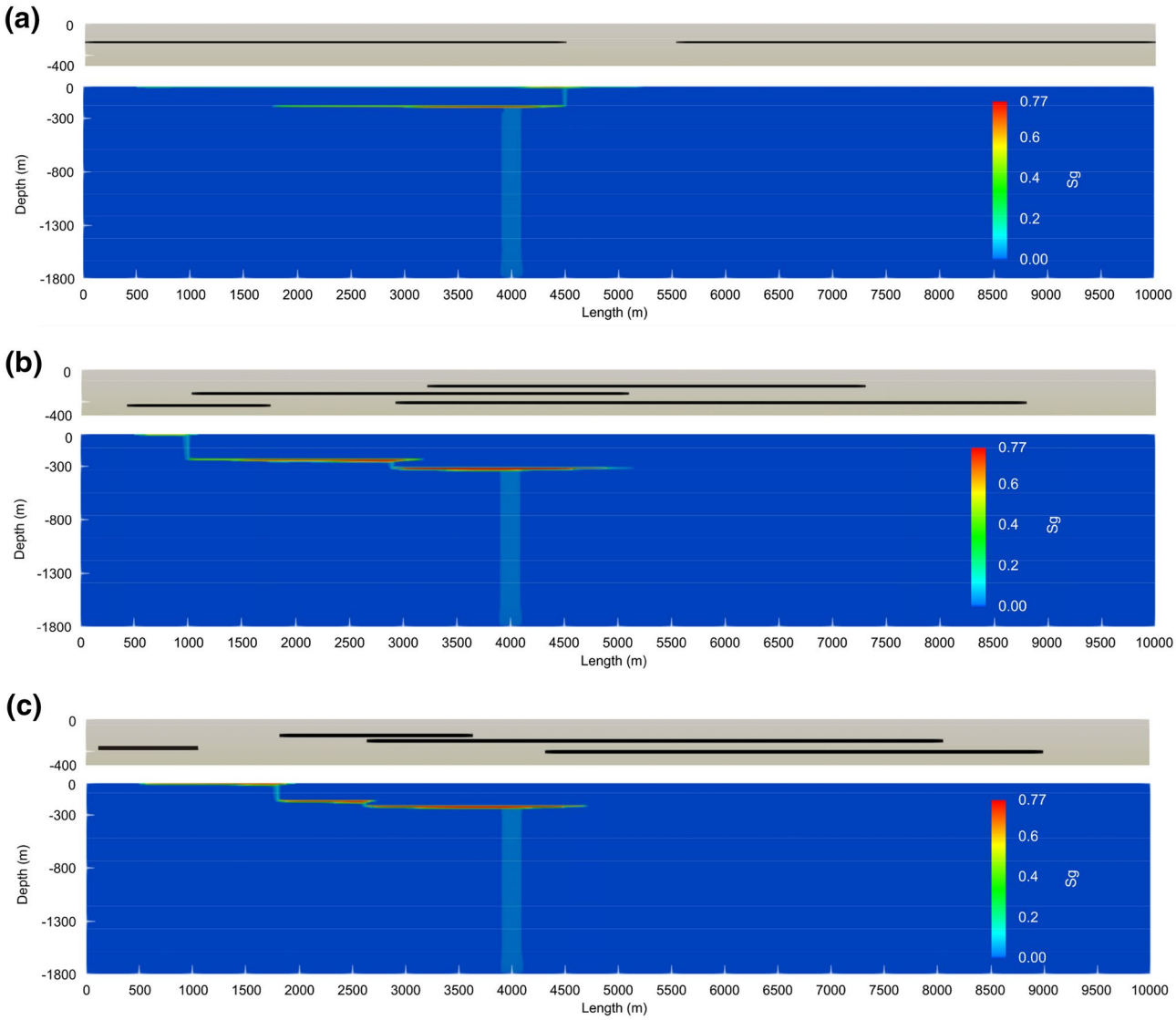

Fig. 10 Gas-phase saturation profiles after 15 years of methane leakage into the overburden. The influence of: **a** claystone layer integrity and different multi-layered claystone systems (**b** case I and **c** case II) is being analyzed. The top panels show the geometry of the claystone layers at shallow depths, in black color

hydrocarbon reservoir into the shallow subsurface. The presence of connective permeable pathways, e.g., faults, interconnected bedding planes, and fractures, in the vicinity of the leaky gas well could result in an early manifestation of methane in groundwater wells (Gorody 2012; Darrah et al. 2014; Cahill et al. 2017). For the leaked methane encountering low-permeability layers, methane preferentially flows along higher permeability sediments, either up-dip (Fig. 9d) or in the direction of groundwater flow (Fig. 10b, c) (Steelman et al. 2017). For such conditions, methane can reach distances of hundreds of meters from the leaky well, delaying the breakthrough to the shallow aquifer system.

Elevated levels of methane concentrations have been observed in groundwater wells within approximately 1 km distance to hydrocarbon wells (Osborn et al. 2011; Jackson et al. 2013; Darrah et al. 2014; Brantley et al. 2014; Heilweil et al. 2015). Our results show that methane can be manifested even at distances of larger than 1 km from the leaky well because of the flow deviation along low-permeability rocks.

The temporal and spatial behavior of the methane plume in the subsurface highly depends on the geological and hydrogeological characteristics of the formations overlying the gas reservoir (Steelman et al. 2017; Rice et al. 2018b). The results indicate that methane can migrate to large distances from the source of leakage and, thus, the concentration of the methane in groundwater wells (if at all) can vary considerably with both time and space. Some observational

Content courtesy of Springer Nature, terms of use apply. Rights reserved.

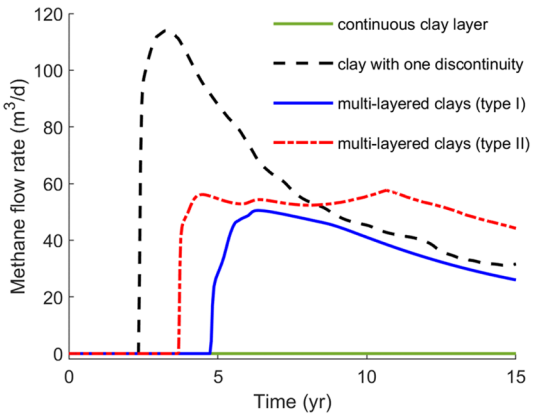

Fig. 11 Methane flow monitored in shallow groundwater for different geometries of claystone layers

studies (Molofsky et al. 2013; Li and Carlson 2014; Siegel et al. 2015; McMahon et al. 2017; Nicot et al. 2017; Botner et al. 2018) found no correlation between thermogenic methane in water samples from groundwater wells and just the distance to hydrocarbon wells corroborating our findings.

Conclusions

We built two-dimensional generic numerical models to assess hydrogeological conditions that could possibly lead to groundwater contamination from the upward migration of methane from leaky natural gas wells. We applied miscible and immiscible multiphase flow models to evaluate the influence of methane solubility on the transport and examine the behavior of methane plume by means of each flow model. Furthermore, we conducted sensitivity analyses to investigate the relative importance of (1) hydrodynamic parameters including entry pressure and pore size distribution index in the Brooks–Corey equation, and residual water saturation, (2) methane leakage rate from the wellbore, (3) tilted formations, and (4) integrity and sequences of claystone layers. The use of relatively simple conceptual models allowed us to provide detailed evaluations on the influence of each parameter studied. Our simulations provide the following insights:

- This study demonstrates that a generic FEP database can be employed for the development of conceptual models representing a potential scenario that may lead to the contamination of shallow groundwater by hydraulic fracturing. The FEP analysis can be used to understand important mechanisms and identify key risks to groundwater resources (Tatomir et al. 2018).
- Miscible and immiscible flow models result in a slightly different temporal and spatial behavior of the plume in the overburden due to the relatively low solubility of methane in the aqueous phase. Methane solubility has a minimal impact on the transport, especially at shallow depths.
- Gas leakage rate and leakage period are among the most important factors controlling the magnitude of methane migration to shallow depths. The persistent long-term leakage leads to the accumulation of large amounts of methane in the overburden, which could potentially be transported into the shallow aquifer system. A pulse of high methane flux is required to generate methane contamination in shallow groundwater for short times; for instance, methane arrival times at the measuring location at a horizontal distance of 2000 m from the leakage source were 11.3 and 5.7 years for the continuous inflow rate of 120 m^3/day and the base-case model, respectively. Results indicate that long-term methane leakage poses higher risks to groundwater in comparison to the rapid migration along fractures (Moortgat et al. 2018) and faults (Reagan et al. 2015) or during drilling operations (Zhang and Soeder 2016).
- The buoyancy component of methane migration can be significant in formations/layers with a sufficient dip angle ($\geq 3°$) in the horizontal and vertical direction. Under such conditions, the presence of low-permeability formations further contributes to the horizontal spreading of the plume and methane can be observed in monitoring wells kilometers away from the leaky well. For example, instances of methane occurrence in groundwater reported in some of observational studies (Molofsky et al. 2013; Li and Carlson 2014; Siegel et al. 2015; McMahon et al. 2017) were not spatially correlated with locations of oil and gas wells, which could further confirm the migration of methane to different distances and directions from the gas well. Our simulations corroborate the results of previous studies that methane observation in groundwater is not concentrically aligned around the leakage source (Jackson et al. 2013; Steelman et al. 2017; Cahill et al. 2017; Rice et al. 2018a; Moortgat et al. 2018; Botner et al. 2018).
- The low-permeability layer, i.e., claystone, is assumed to be horizontal. In reality, such layers may contain dome-shaped and wave-like patterns, similar to surface roughness at the pore-scale level. These structures may retain stratigraphically large portions of the leaked methane. Therefore, the overall contamination may be limited where the lateral extent of the low-permeability layer is larger than a few kilometers. Furthermore, mapping of such features is difficult and future models can be directed at investigating such effects.
- In all modeled scenarios with a continuous claystone at shallow depth, the claystone constitutes an effective flow barrier. Simulations demonstrate that methane can be trapped at the base of a low-permeability unit and spread

Content courtesy of Springer Nature, terms of use apply. Rights reserved.

laterally until it reaches a discontinuity or a permeable vertically oriented pathway. Time to breakthrough and flow rates of methane to monitoring wells can vary strongly depending on the integrity, depth, and distribution of low-permeability sediments with respect to the gas well. For example, in the scenario with a discontinuity in the center of the claystone (Fig. 10a), methane is observed in groundwater within 1 km radius around the well, while in scenarios with multiple claystone layers (Fig. 10b, c), methane is observed at a distance of more than 2 km from the gas well. Our simulations indicate that the complex shape of the methane plume in the subsurface, the arrival time to groundwater (in case of occurrence), and distances from a leaky gas well vary significantly based on hydrogeological characteristics of formations intercalated between aquifer and gas reservoir (Osborn et al. 2011; Jackson et al. 2013; Darrah et al. 2014; Steelman et al. 2017; Cahill et al. 2017; Botner et al. 2018).

Acknowledgements We acknowledge the funding received from the European Union's Horizon 2020 Research and Innovation program. Project "Furthering the knowledge Base for Reducing the Environmental Footprint of Shale Gas Development" FracRisk, Grant agreement 636811. The authors would like to thank the editor, Olaf Kolditz, and the anonymous reviewers for their fruitful and detailed comments that greatly improved the final version of this article.

Funding Open Access funding enabled and organized by Projekt DEAL.

Open Access This article is licensed under a Creative Commons Attribution 4.0 International License, which permits use, sharing, adaptation, distribution and reproduction in any medium or format, as long as you give appropriate credit to the original author(s) and the source, provide a link to the Creative Commons licence, and indicate if changes were made. The images or other third party material in this article are included in the article's Creative Commons licence, unless indicated otherwise in a credit line to the material. If material is not included in the article's Creative Commons licence and your intended use is not permitted by statutory regulation or exceeds the permitted use, you will need to obtain permission directly from the copyright holder. To view a copy of this licence, visit http://creativecommons.org/licenses/by/4.0/.

References

Athy LF (1930) Density, porosity, and compaction of sedimentary rocks. Am Assoc Pet Geol Bull 14:1–24. https://doi.org/10.1306/3D93289E-16B1-11D7-8645000102C1865D

Batzle M, Wang Z (1992) Seismic properties of pore fluids. Geophysics 57:1396–1408. https://doi.org/10.1190/1.1443207

Botner EC, Townsend-Small A, Nash DB et al (2018) Monitoring concentration and isotopic composition of methane in groundwater in the Utica Shale hydraulic fracturing region of Ohio. Environ Monit Assess 190:322. https://doi.org/10.1007/s10661-018-6696-1

Brantley SL, Yoxtheimer D, Arjmand S et al (2014) Water resource impacts during unconventional shale gas development: the Pennsylvania experience. Int J Coal Geol 126:140–156. https://doi.org/10.1016/j.coal.2013.12.017

Brooks AN, Corey AT (1964) Hydraulic properties of porous media. Hydrol Pap (Colo State Univ Fort Collins) 3. http://www.citeulike-article-id:711012

Brown SP, Krupnick A, Walls MA (2009) Natural gas: a bridge to a low-carbon future. In: RFF issue brief. Resources for the Future, Washington, DC, pp 9–11

Cahill AG, Steelman CM, Forde O et al (2017) Mobility and persistence of methane in groundwater in a controlled-release field experiment. Nat Geosci 10:289–294. https://doi.org/10.1038/ngeo2919

Carman PC (1937) Fluid flow through granular beds. Trans Inst Chem Eng 15:150–166

Class H (2007) Models for non-isothermal compositional gas-liquid flow and transport in porous media. Habilitation Thesis, University of Stuttgart

D'Aniello A, Fabbricino M, Ducci D, Pianese D (2019) Numerical investigation of a methane leakage from a geothermal well into a shallow aquifer. Groundwater. https://doi.org/10.1111/gwat.12943

Darrah TH, Jackson RB, Vengosh A et al (2015) The evolution of Devonian hydrocarbon gases in shallow aquifers of the northern Appalachian Basin: insights from integrating noble gas and hydrocarbon geochemistry. Geochim Cosmochim Acta 170:321–355. https://doi.org/10.1016/J.GCA.2015.09.006

Darrah TH, Vengosh A, Jackson RB et al (2014) Noble gases identify the mechanisms of fugitive gas contamination in drinking-water wells overlying the Marcellus and Barnett Shales. Proc Natl Acad Sci 111:14076–14081. https://doi.org/10.1073/pnas.1322107111

Daubert TE, Danner RP, Sibul HM, Stebbins CC (1998) Physical and thermodynamic properties of pure chemicals: data compilation. In: DIPPR/AIChE. Taylor & Francis, Washington, DC

Dietrich P, Helmig R, Sauter M et al (2005) Flow and transport in fractured porous media. Springer, Berlin

Duan Z, Mao S (2006) A thermodynamic model for calculating methane solubility, density and gas phase composition of methane-bearing aqueous fluids from 273 to 523 K and from 1 to 2000 bar. Geochim Cosmochim Acta 70:3369–3386. https://doi.org/10.1016/j.gca.2006.03.018

Duan Z, Møller N, Greenberg J, Weare JH (1992a) The prediction of methane solubility in natural waters to high ionic strength from 0 to 250 °C and from 0 to 1600 bar. Geochim Cosmochim Acta 56:1451–1460. https://doi.org/10.1016/0016-7037(92)90215-5

Duan Z, Møller N, Weare JH (1992b) An equation of state for the CH_4–CO_2–H_2O system: II. Mixtures from 50 to 1000 °C and 0 to 1000 bar. Geochim Cosmochim Acta 56:2619–2631. https://doi.org/10.1016/0016-7037(92)90348-M

Duan Z, Møller N, Weare JH (1992c) An equation of state for the CH_4–CO_2–H_2O system: I. Pure systems from 0 to 1000 °C and 0 to 8000 bar. Geochim Cosmochim Acta 56:2605–2617. https://doi.org/10.1016/0016-7037(92)90347-L

Duncan IJ (2015) Does methane pose significant health and public safety hazards? A review. Environ Geosci 22:85–96. https://doi.org/10.1306/eg.06191515005

Edwards RWJ, Celia MA (2018) Shale gas well, hydraulic fracturing, and formation data to support modeling of gas and water flow in shale formations. Water Resour Res 54:3196–3206. https://doi.org/10.1002/2017WR022130

Flemisch B, Darcis M, Erbertseder K et al (2011) DuMux: DUNE for multi-{phase, component, scale, physics, …} flow and transport in porous media. Adv Water Resour 34:1102–1112. https://doi.org/10.1016/J.ADVWATRES.2011.03.007

Content courtesy of Springer Nature, terms of use apply. Rights reserved.

Fuller EN, Schettler PD, Giddings JC (1966) New method for prediction of binary gas-phase diffusion coefficients. Ind Eng Chem 58:18–27. https://doi.org/10.1021/ie50677a007

Gassiat C, Gleeson T, Lefebvre R, McKenzie J (2013) Hydraulic fracturing in faulted sedimentary basins: numerical simulation of potential contamination of shallow aquifers over long time scales. Water Resour Res 49:8310–8327. https://doi.org/10.1002/2013WR014287

Gleeson T, Smith L, Moosdorf N et al (2011) Mapping permeability over the surface of the Earth. Geophys Res Lett 38:L02401. https://doi.org/10.1029/2010GL045565

Gorody AW (2012) Factors affecting the variability of stray gas concentration and composition in groundwater. Environ Geosci 19:17–31. https://doi.org/10.1306/eg.12081111013

Heilweil VM, Grieve PL, Hynek SA et al (2015) Stream measurements locate thermogenic methane fluxes in groundwater discharge in an area of shale-gas development. Environ Sci Technol 49:4057–4065. https://doi.org/10.1021/es503882b

Helmig R (1997) Multiphase flow and transport processes in the subsurface: a contribution to the modeling of hydrosystems. Springer, Berlin

Hendry MJ, Schmeling EE, Barbour SL et al (2017) Fate and transport of shale-derived, biogenic methane. Sci Rep 7:1–9. https://doi.org/10.1038/s41598-017-05103-8

IEA (2018) World energy outlook 2018. Executive summary. https://www.iea.org/reports/world-energy-outlook-2018

Jackson RB, Vengosh A, Darrah TH et al (2013) Increased stray gas abundance in a subset of drinking water wells near Marcellus shale gas extraction. Proc Natl Acad Sci 110:11250–11255. https://doi.org/10.1073/pnas.1221635110

Kissinger A, Helmig R, Ebigbo A et al (2013) Hydraulic fracturing in unconventional gas reservoirs: Risks in the geological system, part 2: modelling the transport of fracturing fluids, brine and methane. Environ Earth Sci 70:3855–3873. https://doi.org/10.1007/s12665-013-2578-6

Kobayashi K (2004) Optimization methods for multiphase systems in the subsurface: application to methane migration in coal mining areas. PhD Thesis,University of Stuttgart

Koch T, Gläser D, Weishaupt K et al (2020) DuMux 3—an open-source simulator for solving flow and transport problems in porous media with a focus on model coupling. Comput Math Appl. https://doi.org/10.1016/j.camwa.2020.02.012

Kozeny J (1927) Uber kapillare leitung der wasser in boden. Sitzungsber Akad Wiss Wien 136:271–306

Lange T, Sauter M, Heitfeld M et al (2013) Hydraulic fracturing in unconventional gas reservoirs: risks in the geological system part 1. Environ Earth Sci 70:3839–3853. https://doi.org/10.1007/s12665-013-2803-3

Li H, Carlson KH (2014) Distribution and origin of groundwater methane in the Wattenberg oil and gas field of northern Colorado. Environ Sci Technol 48:1484–1491. https://doi.org/10.1021/es404668b

Luijendijk E, Gleeson T (2015) How well can we predict permeability in sedimentary basins? Deriving and evaluating porosity-permeability equations for noncemented sand and clay mixtures. Geofluids 15:67–83. https://doi.org/10.1111/gfl.12115

McGlade C, Speirs J, Sorrell S (2013) Unconventional gas—a review of regional and global resource estimates. Energy 55:571–584. https://doi.org/10.1016/J.ENERGY.2013.01.048

McMahon PB, Barlow JR, Engle MA et al (2017) Methane and benzene in drinking-water wells overlying the Eagle Ford, Fayetteville, and Haynesville Shale hydrocarbon production areas. Environ Sci Technol 51:6727–6734. https://doi.org/10.1021/acs.est.7b00746

Melchers C (2009) Methan im südlichen Münsterland: Genese, Migration und Gefahrenpotenzial. Dissertation, Westfälische Wilhelmsuniversität Münster, p 198

Molofsky LJ, Connor JA, McHugh TE et al (2016) Environmental factors associated with natural methane occurrence in the Appalachian basin. Groundwater 54:656–668. https://doi.org/10.1111/gwat.12401

Molofsky LJ, Connor JA, Wylie AS et al (2013) Evaluation of methane sources in groundwater in northeastern Pennsylvania. Groundwater 51:333–349. https://doi.org/10.1111/gwat.12056

Moortgat J, Schwartz FW, Darrah TH (2018) Numerical modeling of methane leakage from a faulty natural gas well into fractured tight formations. Groundwater 56:163–175. https://doi.org/10.1111/gwat.12630

Nicot JP, Mickler P, Larson T et al (2017) Methane occurrences in aquifers overlying the Barnett shale play with a focus on Parker County, Texas. Groundwater 55:469–481. https://doi.org/10.1111/gwat.12508

Nowamooz A, Comeau F-A, Lemieux J-M (2018) Evaluation of the potential for gas leakage along wellbores in the St Lawrence Lowlands basin, Quebec, Canada. Environ Earth Sci 77:303. https://doi.org/10.1007/s12665-018-7483-6

Nowamooz A, Lemieux JM, Molson J, Therrien R (2015) Numerical investigation of methane and formation fluid leakage along the casing of a decommissioned shale gas well. Water Resour Res 51:4592–4622. https://doi.org/10.1002/2014WR016146

Osborn SG, Vengosh A, Warner NR, Jackson RB (2011) Methane contamination of drinking water accompanying gas-well drilling and hydraulic fracturing. Proc Natl Acad Sci 108:8172–8176. https://doi.org/10.1073/pnas.1100682108

Pfunt H, Houben G, Himmelsbach T (2016) Numerical modeling of fracking fluid migration through fault zones and fractures in the North German Basin. Hydrogeol J 24:1343–1358. https://doi.org/10.1007/s10040-016-1418-7

Pitzer KS, Peiper JC, Busey RH (1984) Thermodynamic properties of aqueous sodium chloride solutions. J Phys Chem Ref Data 13:1–102. https://doi.org/10.1063/1.555709

Potter van Loon A (2016) How clay layers control basin-scale fluid and heat flow. Bachelor Thesis, University of Göttingen

Reagan MT, Moridis GJ, Keen ND, Johnson JN (2015) Numerical simulation of the environmental impact of hydraulic fracturing of tight/shale gas reservoirs on near-surface groundwater: background, base cases, shallow reservoirs, short-term gas, and water transport. Water Resour Res 4:2543–2573. https://doi.org/10.1002/2014WR016086

Reid R, Prausnitz J, Poling B (1987) The properties of gases and liquids. McGraw-Hill, New York

Rice AK, Lackey G, Proctor J, Singha K (2018a) Groundwater-quality hazards of methane leakage from hydrocarbon wells: a review of observational and numerical studies and four testable hypotheses. Wiley Interdiscip Rev Water 5:e1283. https://doi.org/10.1002/wat2.1283

Rice AK, McCray JE, Singha K (2018b) Methane leakage from hydrocarbon wellbores into overlying groundwater: numerical investigation of the multiphase flow processes governing migration. Water Resour Res 54:2959–2975. https://doi.org/10.1002/2017WR021365

Riddick SN, Mauzerall DL, Celia MA et al (2019) Measuring methane emissions from abandoned and active oil and gas wells in West Virginia. Sci Total Environ 651:1849–1856. https://doi.org/10.1016/J.SCITOTENV.2018.10.082

Rivard C, Bordeleau G, Lavoie D et al (2019) Assessing potential impacts of shale gas development on shallow aquifers through upward fluid migration: a multi-disciplinary approach applied to

Content courtesy of Springer Nature, terms of use apply. Rights reserved.

the Utica Shale in eastern Canada. Mar Pet Geol 100:466–483. https://doi.org/10.1016/J.MARPETGEO.2018.11.004

Roy N, Molson J, Lemieux JM et al (2016) Three-dimensional numerical simulations of methane gas migration from decommissioned hydrocarbon production wells into shallow aquifers. Water Resour Res 52:5598–5618. https://doi.org/10.1002/2016WR018686

Rudolph T, Melchers C, Minke A, Coldewey WG (2010) Gas seepages in Germany: revisited subsurface permeabilities in the German mining district. Am Assoc Pet Geol Bull 94:847–867. https://doi.org/10.1306/10210909074

Sauter M, Brosig K, Lange T, et al (2012) Risiken im Geologischen System bei der Fracking-Technologie. Abschötzung der Auswirkungen auf Grundwasservorkommen

Schout G, Hartog N, Hassanizadeh SM et al (2020) Impact of groundwater flow on methane gas migration and retention in unconsolidated aquifers. J Contam Hydrol 230:103619. https://doi.org/10.1016/j.jconhyd.2020.103619

Schwartz MO (2015) Modelling the hypothetical methane-leakage in a shale-gas project and the impact on groundwater quality. Environ Earth Sci 73:4619–4632. https://doi.org/10.1007/s12665-014-3787-3

Sclater JG, Christie PAF (1980) Continental stretching: an explanation of the Post-Mid-Cretaceous subsidence of the central North Sea Basin. J Geophys Res Solid Earth 85:3711–3739. https://doi.org/10.1029/JB085iB07p03711

Sherwood OA, Rogers JD, Lackey G et al (2016) Groundwater methane in relation to oil and gas development and shallow coal seams in the Denver-Julesburg Basin of Colorado. Proc Natl Acad Sci 113:8391–8396. https://doi.org/10.1073/PNAS.1523267113

Siegel DI, Azzolina NA, Smith BJ et al (2015) Methane concentrations in water wells unrelated to proximity to existing oil and gas wells in northeastern Pennsylvania. Environ Sci Technol 49:4106–4112. https://doi.org/10.1021/es505775c

Soltanian MR, Amooie MA, Cole DR et al (2018) Impacts of methane on carbon dioxide storage in brine formations. Groundwater 56:176–186. https://doi.org/10.1111/gwat.12633

Steelman CM, Klazinga DR, Cahill AG et al (2017) Monitoring the evolution and migration of a methane gas plume in an unconfined sandy aquifer using time-lapse GPR and ERT. J Contam Hydrol 205:12–24. https://doi.org/10.1016/j.jconhyd.2017.08.011

Taherdangkoo R, Luijendijk E, Potter van Loon A, Gleeson T (2018) How clay layers control basin-scale fluid and heat flow. In: 20th EGU general assembly, EGU2018, 4–13 April. Vienna, Austria, p 12350

Taherdangkoo R, Tatomir A, Anighoro T, Sauter M (2019) Modeling fate and transport of hydraulic fracturing fluid in the presence of abandoned wells. J Contam Hydrol 221:58–68. https://doi.org/10.1016/j.jconhyd.2018.12.003

Tatomir A, McDermott C, Bensabat J et al (2018) Conceptual model development using a generic features, events, and processes (FEP) database for assessing the potential impact of hydraulic fracturing on groundwater aquifers. Adv Geosci 45:185–192. https://doi.org/10.5194/adgeo-45-185-2018

Tatomir A, McDermott C, Edlmann K et al (2015) D3.1 Update of FEP database (version 2)

U.S. EPA (2015) Assessment of the potential impacts of hydraulic fracturing for oil and gas on drinking water resources (external review draft). U.S. EPA: Washington, DC

Vengosh A, Jackson R, Warner N (2014) A critical review of the risks to water resources from unconventional shale gas development and hydraulic fracturing in the United States. Environ Sci Technol 48:8334–8348. https://doi.org/10.1021/es405118y

Warner NR, Jackson RB, Darrah TH et al (2012) Geochemical evidence for possible natural migration of Marcellus Formation brine to shallow aquifers in Pennsylvania. Proc Natl Acad Sci USA 109:11961–11966. https://doi.org/10.1073/pnas.1121181109

Weibel R, Kristensen L, Olivarius M et al (2012) Investigating deviations from overall porosity–permeability trends. In: Proceedings 36th workshop on geothermal reservoir engineering, Stanford University, California, vol 16

Yudhowijoyo A, Rafati R, Sharifi Haddad A et al (2018) Subsurface methane leakage in unconventional shale gas reservoirs: a review of leakage pathways and current sealing techniques. J Nat Gas Sci Eng 54:309–319. https://doi.org/10.1016/J.JNGSE.2018.04.013

Zhang L, Soeder DJ (2016) Modeling of methane migration in shallow aquifers from shale gas well drilling. Groundwater 54:345–353. https://doi.org/10.1111/gwat.12361

Publisher's Note Springer Nature remains neutral with regard to jurisdictional claims in published maps and institutional affiliations.

Content courtesy of Springer Nature, terms of use apply. Rights reserved.

Terms and Conditions

Springer Nature journal content, brought to you courtesy of Springer Nature Customer Service Center GmbH ("Springer Nature").

Springer Nature supports a reasonable amount of sharing of research papers by authors, subscribers and authorised users ("Users"), for small-scale personal, non-commercial use provided that all copyright, trade and service marks and other proprietary notices are maintained. By accessing, sharing, receiving or otherwise using the Springer Nature journal content you agree to these terms of use ("Terms"). For these purposes, Springer Nature considers academic use (by researchers and students) to be non-commercial.

These Terms are supplementary and will apply in addition to any applicable website terms and conditions, a relevant site licence or a personal subscription. These Terms will prevail over any conflict or ambiguity with regards to the relevant terms, a site licence or a personal subscription (to the extent of the conflict or ambiguity only). For Creative Commons-licensed articles, the terms of the Creative Commons license used will apply.

We collect and use personal data to provide access to the Springer Nature journal content. We may also use these personal data internally within ResearchGate and Springer Nature and as agreed share it, in an anonymised way, for purposes of tracking, analysis and reporting. We will not otherwise disclose your personal data outside the ResearchGate or the Springer Nature group of companies unless we have your permission as detailed in the Privacy Policy.

While Users may use the Springer Nature journal content for small scale, personal non-commercial use, it is important to note that Users may not:

1. use such content for the purpose of providing other users with access on a regular or large scale basis or as a means to circumvent access control;
2. use such content where to do so would be considered a criminal or statutory offence in any jurisdiction, or gives rise to civil liability, or is otherwise unlawful;
3. falsely or misleadingly imply or suggest endorsement, approval , sponsorship, or association unless explicitly agreed to by Springer Nature in writing;
4. use bots or other automated methods to access the content or redirect messages
5. override any security feature or exclusionary protocol; or
6. share the content in order to create substitute for Springer Nature products or services or a systematic database of Springer Nature journal content.

In line with the restriction against commercial use, Springer Nature does not permit the creation of a product or service that creates revenue, royalties, rent or income from our content or its inclusion as part of a paid for service or for other commercial gain. Springer Nature journal content cannot be used for inter-library loans and librarians may not upload Springer Nature journal content on a large scale into their, or any other, institutional repository.

These terms of use are reviewed regularly and may be amended at any time. Springer Nature is not obligated to publish any information or content on this website and may remove it or features or functionality at our sole discretion, at any time with or without notice. Springer Nature may revoke this licence to you at any time and remove access to any copies of the Springer Nature journal content which have been saved.

To the fullest extent permitted by law, Springer Nature makes no warranties, representations or guarantees to Users, either express or implied with respect to the Springer nature journal content and all parties disclaim and waive any implied warranties or warranties imposed by law, including merchantability or fitness for any particular purpose.

Please note that these rights do not automatically extend to content, data or other material published by Springer Nature that may be licensed from third parties.

If you would like to use or distribute our Springer Nature journal content to a wider audience or on a regular basis or in any other manner not expressly permitted by these Terms, please contact Springer Nature at

onlineservice@springernature.com